Title: Dbx1 pre-Bötzinger complex interneurons comprise the core inspiratory oscillator for breathing in adult mice

Authors: Nikolas C. Vann, Francis D. Pham, Kaitlyn E. Dorst, and Christopher A. Del Negro

Author affiliation: Department of Applied Science, The College of William and Mary, Williamsburg, VA 23185

Nikolas C. Vann ORCID: 0000-0003-4139-0642

Francis D. Pham ORCID: 0000-0003-1082-8533

Kaitlyn Dorst ORCID: 0000-0002-5393-2608

Christopher A. Del Negro ORCID: 0000-0002-7848-8224

Corresponding author: Christopher A. Del Negro, Ph.D., Professor and Chair, Department of Applied Science, Integrated Science Center, 540 Landrum Dr., The College of William and Mary, Williamsburg, Virginia, 757-221-7808 (office), 757-221-2050 (fax), cadeln@wm.edu

Conflict of interest: The authors declare no competing financial interests.

Acknowledgements: National Institutes of Health grant R01 HL104127 (PI: Del Negro) supported this work.

ABSTRACT

The brainstem pre-Bötzinger complex (preBötC) generates inspiratory breathing rhythms, but which neurons comprise its rhythmogenic core? Dbx1-derived neurons may play the preeminent role in rhythm generation, an idea well founded at perinatal stages of development but not in adulthood. We expressed archaerhodopsin or channelrhodopsin in Dbx1 preBötC neurons in intact adult mice to interrogate their function. Prolonged photoinhibition slowed down or stopped breathing, whereas prolonged photostimulation sped up breathing. Brief inspiratory-phase photoinhibition evoked the next breath earlier than expected, whereas brief expiratory-phase photoinhibition delayed the subsequent breath. Conversely, brief inspiratory-phase photostimulation increased inspiratory duration and delayed the subsequent breath, whereas brief expiratory-phase photostimulation evoked the next breath earlier than expected. Because they govern the frequency and precise timing of breaths in awake adult mice with sensorimotor feedback intact, Dbx1 preBötC neurons constitute an essential core component of the inspiratory oscillator, knowledge directly relevant to human health and physiology.

INTRODUCTION

Inspiratory breathing movements in mammals originate from neural rhythms in the brainstem preBötzinger Complex (preBötC) (Feldman et al., 2013; Smith et al., 1991). Although the preBötC has been identified in a range of mammals including bats, moles, goats, cats, rabbits, rats, mice, and humans (Mutolo et al., 2002; Pantaleo et al., 2011; Ruangkittisakul et al., 2011; Schwarzacher et al., 1995, 2010; Smith et al., 1991; Tupal et al., 2014; Wenninger et al., 2004) its neuronal constituents remain imprecise. Competing classification schemes emphasize peptide and peptide receptor expression (Gray et al., 1999, 2001; Stornetta et al., 2003a; Tan et al., 2008) as well as a glutamatergic transmitter phenotype (Funk et al., 1993; Stornetta et al., 2003b; Wallen-Mackenzie et al., 2006) as cellular markers that define the preBötC rhythmogenic core.

Interneurons derived from precursors that express the homeodomain transcription factor Dbx1 (i.e., Dbx1 neurons) also express peptides and peptide receptors associated with respiratory rhythmogenesis, and are predominantly glutamatergic. *Dbx1* knock-out mice die at birth of asphyxia and the preBötC never forms (Bouvier et al., 2010; Gray et al., 2010). In rhythmically active slice preparations from neonatal Dbx1 reporter mice, Dbx1 preBötC neurons discharge in bursts in phase with inspiration (Picardo et al., 2013), and their sequential laser ablation slows

and then stops respiratory motor output (Wang et al., 2014). These results obtained from perinatal mice suggest that Dbx1 neurons comprise the rhythmogenic preBötC core, i.e., the Dbx1 core hypothesis.

Nevertheless, in addition to their putatively rhythmogenic role, Dbx1 preBötC neurons also govern motor pattern. Hypoglossal motoneurons that maintain airway patency receive rhythmic synaptic drive from Dbx1 neurons within the preBötC and adjacent intermediate reticular formation (Revill et al., 2015; Song et al., 2016; Wang et al., 2014). In anesthetized vagotomized adult mice, photostimulation of Dbx1 preBötC neurons modulates inspiratory timing and its motor pattern, which is mediated in part by somatostatin-expressing (Sst) preBötC neurons (Cui et al., 2016), a large fraction of which are derived from Dbx1-expressing progenitors (Bouvier et al., 2010; Gray et al., 2010; Koizumi et al., 2016).

In adult animals, Dbx1 preBötC neurons serve non-respiratory roles as well. A subset that expresses Cadherin-9 (Cdh9) projects to the pontine locus coeruleus to influence arousal (Yackle et al., 2017). Collectively, the fractions of motor output-related (Sst-expressing) and arousal-related (Cdh9-expressing) Dbx1 neurons could account for 73% of Dbx1 neurons within the preBötC: up to 17% of Dbx1 preBötC neurons express Sst and 56% express Cdh9 with no overlap between Sst and Cdh9 expression (Bouvier et al., 2010; Cui et al., 2016; Gray et al., 2010; Yackle et al., 2017). That accounting would leave 27% of Dbx1 preBötC neurons exclusively rhythmogenic, if one assumes that all remaining Dbx1 neurons are dedicated to respiration and that single Dbx1 preBötC neurons cannot fulfill multiple duties. Therefore, while their rhythmogenic role is well established at perinatal stages of development (Bouvier et al., 2010; Gray et al., 2010), the contemporary studies recapped above from adult mice imply that rhythm generation may not be the principal function of Dbx1 preBötC neurons.

Here we reevaluate the inspiratory rhythmogenic role of Dbx1 preBötC neurons in adult mice with intact sensorimotor feedback. Using optogenetic technologies to photoinhibit or photostimulate Dbx1 neurons, we show that their perturbation affects breathing frequency and the precise timing of individual breaths within the breathing cycle, which are key properties of a core oscillator microcircuit. Other respiratory and non-respiratory roles notwithstanding, these data indicate that Dbx1 preBötC neurons constitute an essential core oscillator for inspiration.

RESULTS

ArchT activation hyperpolarizes Dbx1 preBötC neurons postsynaptically

We illuminated the preBötC in transverse medullary slices from neonatal Dbx1;ArchT mice (the intersection of a *Dbx1*^{CreERT2} driver mouse and a reporter featuring Cre-dependent archaerhodopsin [ArchT] expression) that spontaneously generate inspiratory rhythm and airway-related hypoglossal (XII) motor output. Light application (589 nm) to the preBötC bilaterally stopped rhythm and motor output at all light intensities (Figure 1 – figure supplement 1A and B). Dbx1 preBötC neurons recorded in whole-cell patch-clamp hyperpolarized 6.5 ± 1.0, 8.1 ± 1.1, and 11.0 ± 2.5 mV in response to light of increasing intensity (Figure 1A, cyan). We reapplied the highest intensity light in the presence of TTX, which hyperpolarized Dbx1 preBötC neurons by 8.6 ± 1.4 mV (Figure 1A and B, cyan). Light-evoked hyperpolarization was commensurate before and after TTX (Mann-Whitney U, $p = 0.2$, $n_1 = 8$, $n_2 = 3$), which suggests that ArchT hyperpolarizes Dbx1 preBötC neurons via direct postsynaptic effects.

In the same slices from neonatal Dbx1;ArchT mice, we illuminated the preBötC bilaterally while patch recording neighboring non-Dbx1 preBötC neurons. Baseline membrane potential in non-Dbx1 preBötC neurons responded negligibly to light, hyperpolarizing 0.7 ± 0.3, 1.1 ± 0.5, and 1.1 ± 0.6 mV in response to light of increasing intensity (Figure 1A, magenta, and Figure 1 – figure supplement 1B). In TTX, light at the highest intensity hyperpolarized non-Dbx1 neurons by 0.3 ± 0.8 mV (Figure 1A and B, magenta), which was indistinguishable from light-evoked hyperpolarization before TTX application (Mann-Whitney U, $p = 0.2$, $n_1 = 8$, $n_2 = 4$). These results suggest that light-evoked cessation of inspiratory rhythm and motor output *in vitro* is largely attributable to direct postsynaptic effects on Dbx1 preBötC neurons rather than network disfacilitation, which would comparably affect Dbx1 as well as non-Dbx1 neurons in the preBötC and would be eliminated by TTX.

Photoinhibition of Dbx1 preBötC neurons attenuates breathing and resets inspiration

Next we illuminated the preBötC bilaterally using fiberoptic implants (Figure 1C shows tracks of fiberoptics in post-hoc histology) in sedated adult Dbx1;ArchT mice, which reduced breathing in all instances (Figure 2A). In control conditions breathing frequency (f) was typically ~3.5 Hz, tidal volume (V_T) was ~0.1 ml, and minute ventilation (MV) was ~50 ml/min. The lowest intensity light (6.8 mW) decreased f by 0.3 Hz (t-test, $p = 0.05$, $n = 6$), decreased V_T by 0.2 ml (but that

change was not statistically significant by t-test, p = 0.06, n = 6), and decreased MV by 9 ml/min (t-test, p = 0.01, n = 6) (Figure 2B).

f, V_T, and MV decreased to a greater extent in response to 8.6 and 10.2 mW intensity illumination (Figure 2A). f decreased by 1.2 and 2.0 Hz, respectively (t-test, p = 0.001 and p = 0.0001, n = 6). Apnea – no inspiratory effort – resulted in more than one-third of all trials at 10.2 mW (i.e., 11 of 30 bouts, e.g., Figure 2A, bottom). V_T decreased in response to 8.6 and 10.2 mW light in both cases by 0.03 ml (t-test, p = 0.04 and p = 0.02, n = 6). MV decreased by 11 and 20 ml/min, respectively (t-test, both p = 0.02, n = 6) (Figure 2B).

In comparison, sedated wild-type littermates subjected to the same protocol showed no light-evoked changes in breathing (Figure 2 – figure supplement 1A and 1B).

We repeated these experiments in Dbx1;ArchT mice while awake and unrestrained (Figure 2C). The lowest intensity light (6.8 mW) decreased f and V_T by 0.01 Hz and 0.03 ml, respectively (neither change was statistically significant by t-test, p = 0.06 and 0.07, n = 5). MV decreased significantly by 7.4 ml/min (t-test, p = 0.04, n = 5) (Figure 2D).

The effects on breathing were more profound when we illuminated at 8.6 and 10.2 mW (Figure 2C). f decreased by 1.1 and 1.2 Hz, respectively (t-test, p = 0.002 and p = 0.02, n = 5) and MV decreased by 22 and 32 ml/min, respectively (t-test, p = 0.04 and p = 0.03, n = 5). One animal stopped breathing for ~4 s (i.e., apnea, Figure 2C, bottom trace). Although V_T decreased by 0.05 and 0.15 ml, respectively, statistical hypothesis testing did not detect significant light-induced changes (t-test, p = 0.2 and p = 0.08, n = 5), probably due to the high variability of V_T in awake animals (Figure 2D).

In comparison, awake unrestrained wild-type littermates showed no changes in breathing in reponse to light of any intensity (Figure 2 – figure supplement 1C and 1D).

Therefore, these data collectively show that ArchT-mediated Dbx1 preBötC neuron hyperpolarization reduces breathing up to and including apnea in sedated and awake intact mice.

Next we applied brief (100 ms) light pulses randomly during the breathing cycle, which we defined as spanning 0-360º (see Materials and Methods, Figure 3 inset). Brief photoinhibition of the preBötC early during inspiration (Φ_{Stim} of 0-30º) caused a phase advance such that the

subsequent inspiration occurred earlier than expected (Φ_{Shift} = -147 ± 23º, p = 1e-6, n = 4) while shortening inspiratory time (T_i) by almost half (ΔT_i = 45 ± 5%, p = 1e-6, n = 4) (Figure 3$A_{1,2}$ and A_3 top trace). Brief photoinhibition also evoked significant phase advances and reduced T_i during the rest of inspiration (Φ_{Stim} of 30-120º), but the magnitude of those changes monotonically decreased as Φ_{Stim} approached the inspiratory-expiratory transition.

Brief photoinhibition did not perturb the system during the inspiratory-expiratory transition (Φ_{Stim} of 120-180º). During early expiration (Φ_{Stim} of 180-210º), which is often referred to as post-inspiration (Anderson et al., 2016; Dutschmann et al., 2014) we observed the first significant phase delay such that the subsequent inspiration occurred later than expected in response to brief photoinhibition (Φ_{Shift} = 32 ± 7º, p = 0.006, n = 4, Figure 3A_1 and A_3 bottom trace). Phase delays were consistently evoked during expiration (Φ_{Stim} of 210-360º) with a maximum phase delay during late expiration (Φ_{Stim} of 300-330º) (Φ_{Shift} = 78 ± 10º, p = 1e-6, n = 4). Brief photoinhibition during expiration did not affect T_i, which is a straightforward result because the inspiratory period had ended (Figure 3A_2). Note, that ΔT_i was statistically significant at Φ_{Stim} of 210-240º) but that change is not physiologically meaningful because the magnitude of the change is small and not part of a consistent trend in the phase-response curve.

The relationship between Φ_{Stim} and the phase of the subsequent breath (Φ_{N+1}, Figure 3 – figure supplement 1A_1) closely resembled the relationship between Φ_{Stim} and Φ_{Shift} (Figure 3A_1), which suggests that brief photoinhibition resets the phase of the oscillator.

In contrast to its effects on breathing phase (Φ_{Shift} and Φ_{N+1}), brief photoinhibition had little effect on V_T throughout most of the respiratory cycle with changes of less than 10% across the entire respiratory cycle, except during early inspiration (Φ_{Stim} of 0-30º, in which V_T decreased by 23 ± 8%, p = 0.02, n = 4) and early expiration (Φ_{Stim} of 150-180º, in which V_T increased by 16 ± 11%, p = 0.01, n = 4) (Figure 3 – figure supplement 1A_2). Despite the fact that two out of 12 measurements pass the threshold for statistical significance, these data do not convincingly demonstrate that brief photoinhibition of Dbx1 preBötC neurons systematically influences V_T in sedated mice.

We repeated brief photoinhibition experiments in awake unrestrained Dbx1;ArchT mice. The plots of Φ_{Shift}, ΔT_i, Φ_{N+1}, and ΔV_T versus Φ_{Stim} were qualitatively similar to the experiments in sedated mice (compare Figure 3A to 3B and Figure 3 – figure supplement 1A to 1B). Photoinhibition during early inspiration (Φ_{Stim} of 0-30º) caused a phase advance (Φ_{Shift} = -86 ±

16º, p = 1e-5, n = 4). The first significant phase delay in the awake animal occurred when brief photoinhibition was applied during peak expiration (Φ_{Stim} of 210-240º, Φ_{Shift} = 68 ± 15º, p = 1e-6, n = 4). Φ_{Shift} tended to increase as brief photoinhibition was applied at later points during the expiratory phase. The maximum phase delay occurred during late expiration (Φ_{Stim} of 330-360º, Φ_{Shift} = 118 ± 25º, p = 4e-5, n = 4) (Figure 3B_1 and B_3). Brief photoinhibition decreased T_i by nearly one-third (ΔT_i = 28 ± 9%, p = 1e-5, n = 4) during early inspiration (Φ_{Stim} of 0-30º) but had no significant effect at any other time during the cycle.

Photostimulation of Dbx1 preBötC neurons enhances breathing and modifies the timing and magnitude of breaths

We illuminated the preBötC unilaterally in sedated adult Dbx1;CatCh mice (the intersection of a *Dbx1*^{CreERT2} driver mouse and a reporter featuring Cre- and Flp-dependent calcium translocating channelrhodopsin [CatCh] expression) following viral transduction in the preBötC with a synapsin-driven Flp recombinase. Using this double-stop intersectional approach, CatCh-EYFP expression was limited to the preBötC (Figure 1D). In control conditions f was typically ~3 Hz, V_T was ~0.1 ml, and MV was ~50 ml/min. Bouts of blue light (473 nm) at three intensities significantly increased f by 0.8, 1.1, and 1.3 Hz, respectively (t-test, p = 0.03, 0.005, and 0.03, n = 4). There were no significant effects on V_T or MV at any light intensity (Figure 4A and B).

We repeated these unilateral photostimulation experiments in Dbx1;CatCh mice while awake and unrestrained. Frequency increased by 1.6 Hz in response to light at the highest intensity (Figure 4C and D). There were no other notable changes in f, V_T, or MV at any light intensity.

In wild type littermates, we observed no effects on breathing in either sedated or awake mice in response to light at any intensity (Figure 4 – figure supplement 1).

Therefore, these data collectively show that CatCh-mediated photostimulation of Dbx1 preBötC neurons selectively enhances breathing frequency in sedated and awake intact mice.

Next we applied brief (100 ms) light pulses at different time points during the breathing cycle. Unilateral illumination of the preBötC during inspiration caused a phase delay and increased T_i. The maximum phase delay occurred during peak inspiration (Φ_{Stim} of 60-90º, Φ_{Shift} = 125 ± 18º, p = 1e-6, n = 4) (Figure 5A_1) and coincided with the maximum ΔT_i (29 ± 7%, p = 1e-6, n = 4) (Figure 5A_2). Brief photostimulation caused a phase advance during the inspiratory-expiratory transition (Φ_{Stim} of 90-120º) and throughout expiration ($\Phi_{Stim} \geq$ 120º) without affecting T_i. The

maximum phase advance occurred during early expiration (Φ_{Stim} of 150-180º, Φ_{Shift} = -128 ± 4º, p = 1e-6, n = 4) (Figure 5A$_1$ and A$_3$). The relationship between Φ_{Stim} and the phase of the subsequent breath (Φ_{N+1}, Figure 5 – figure supplement 1A$_1$) mimicked the relationship between Φ_{Stim} and Φ_{Shift} (Figure 5A$_1$), which suggests that brief photostimulation resets the phase of the oscillator. We observed no effects of brief photostimulation on V_T (Figure 5 – figure supplement 1A$_2$).

We repeated brief photostimulation experiments in awake intact Dbx1;CatCh mice. The plots of Φ_{Shift} and ΔT_i vs Φ_{Stim} were qualitatively similar to those recorded in sedated mice (compare Figure 5B to 5A). Brief photostimulation during early and mid-inspiration (Φ_{Stim} of 0-60º) caused a phase delay (maximum Φ_{Shift} = 147 ± 52, p = 1e-5, n = 4) (Figure 5B$_1$). We measured no phase shift for late inspiration (Φ_{Stim} of 60-90º). The phasic effect of brief photostimulation changed sign around the inspiratory-expiratory transition ($\Phi_{Stim} \geq$ 90º); brief photostimulation subsequently evoked breaths earlier than expected. We measured the maximum phase advance during early expiration (Φ_{Stim} of 120-150º, Φ_{Shift} = -159 ± 9º, p = 1e-5, n = 4) (Figure 5B$_1$). The last statistically significant phase delay occurred during late expiration (Φ_{Stim} of 270-300º, Φ_{Shift} = -52 ± 3º, p = 0.05, n = 4).

Brief photostimulation of Dbx1 preBötC neurons in awake intact mice also extended T_i during inspiration (Figure 5B$_2$); the effect was even more pronounced than in sedated mice (Figure 5A$_2$). The maximum ΔT_i occurred during early inspiration (Φ_{Stim} of 0-30º) in which T_i increased by over half (56 ± 14%, p = 1e-6, n = 4). The ability of brief photostimulation to extend T_i decreased during the inspiratory phase (Figure 5B$_1$) such that no significant effects occurred after Φ_{Stim} exceeded 90º. The relationship between Φ_{Stim} and Φ_{N+1} illustrated a phase delay evoked by brief photostimulation during mid-inspiration (Φ_{Stim} of 30-60º, Figure 5 – figure supplement 1A$_1$), which partially recaps the relationship that was more pronounced in the plot of Φ_{Shift} vs. Φ_{Stim} (Figure 5A$_1$). We observed no relationship for ΔV_T vs. Φ_{Stim} (Figure 5 – figure supplement 1B$_2$), as in the sedated mouse (Figure 5 – figure supplemnt 1B$_1$).

These data are consistent photostimulus-induced resetting of the inspiratory oscillator, although the data are noisier in the awake adult, freely behaving mouse.

DISCUSSION

Role diversity challenges the Dbx1 core hypothesis

The idea that Dbx1 preBötC neurons are inspiratory rhythmogenic has become generally well accepted, but it must be reevaluated given the expanding spectrum of non-rhythmogenic and non-respiratory functions attributed to this neuron class, particularly in adult animals.

Perinatally Dbx1 preBötC neurons generate rhythm and pattern. *Dbx1* knock-out mice do not breathe and form no recognizable preBötC (Bouvier et al., 2010; Gray et al., 2010), the site of inspiratory rhythmogenesis (Del Negro et al., 2018; Feldman and Del Negro, 2006; Feldman et al., 2013; Ramirez et al., 2016; Smith et al., 1991). Their selective destruction in a slice model of breathing (Funk and Greer, 2013) slows and then stops the rhythm, evidence of their rhythmogenic role, while also attenuating airway-related XII motor output (Wang et al., 2014) because of Dbx1 premotor neurons in the preBötC that drive XII (Revill et al., 2015; Wang et al., 2014) as well as phrenic motoneurons (Wu et al., 2017).

This theme continues in adult mice. Sst-expressing preBötC neurons, ~17% of the Dbx1-derived population, appear to lack rhythmogenic function but rather shape motor output pattern (Cui et al., 2016), q.v., (Koizumi et al., 2016). More than half (56%) of Dbx1 preBötC neurons characterized by Cdh9 expression lack respiratory rhythmicity but project to the locus coeruleus and putatively influence arousal (Yackle et al., 2017). If we assume that non-Sst and non-Cdh9 Dbx1 neurons have respiratory functions, and that individual neurons do not fulfill multiple duties, then these statistics suggest that not more than 27% of Dbx1 preBötC neurons in adult mice are exclusively rhythmogenic.

Photoinhibition and photostimulation demonstrate Dbx1 preBötC neurons influence rhythm and pattern

Sustained photoinhibition caused graded frequency decreases including apnea, which are evidence that Dbx1 neurons form the core oscillator. However, photoinhibition also decreased V_T, indicating that Dbx1 neurons also govern breath size, i.e., motor pattern. We reported qualitatively similar data in (Vann et al., 2016) but the effects were more mild because of the weaker archaerhodopsin variant available at the time. Dbx1 neurons that influence airway and pump-related motor function have been analyzed in detail (Cui et al., 2016; Revill et al., 2015; Wang et al., 2014; Wu et al., 2017). Here we limit our comments to acknowledging those motor-

255 related roles, and we concentrate on analyzing the role of Dbx1 preBötC neurons in
256 rhythmogenesis.

257 Sustained photostimulation approximately doubled the breathing rate from ~3.5 to 7 Hz. In
258 contrast, Baertsch and colleagues (Baertsch et al., 2018) reported minor (~10%) frequency
259 changes in vagus intact mice in response to sustained photostimulation. These two results are
260 not discrepant, even if they appear to be at face value. We were able to evoke higher
261 frequencies in our experiments most likely due to the accelerated response time, enhanced light
262 sensitivity, larger voltage responses evoked by photoactivated CatCh compared to ChR2
263 (Kleinlogel et al., 2011), and the fact that we applied laser strengths up to 10.2 mW whereas
264 Baertsch *et al.* purposely limited their pulses to 7 mW or less (Baertsch et al., 2018). Those
265 authors showed that phasic synaptic inhibition critically influences breathing frequency and we
266 do not disagree. We purposely did not vagotomize our mice to preserve phasic synaptic
267 inhibition and thus high breathing frequencies are possible during photostimulation.

268 ***Phase-response experiments demonstrate that Dbx1 preBötC neurons are rhythmogenic***

269 If Dbx1 preBötC neurons are inspiratory rhythmogenic, then transiently stimulating them should
270 evoke inspiratory breaths at any point in the breathing cycle except, potentially, during the post-
271 inspiratory (early expiratory) refractory period identified *in vitro* (Guerrier et al., 2015; Kottick and
272 Del Negro, 2015) and in vagotomized mice *in vivo* (Baertsch et al., 2018). We evoked
273 inspiratory breaths at all points during the respiratory cycle without evidence of a refractory
274 period. Brief photostimulation during inspiration prolonged it (i.e., increased T_i) and delayed the
275 next cycle (i.e., a phase delay). The straightforward interpretation is that CatCh-mediated inward
276 current augments recurrent excitation thus prolonging inspiratory burst duration. Overexcited
277 rhythmogenic neurons require more time to recover, which lengthens cycle time and delays the
278 subsequent inspiration.

279 We observed that photostimulation at any other point in the cycle evoked inspiration earlier than
280 expected, a phase advance, but did not otherwise modify inspiration. In contrast to a prior
281 report, brief photostimulation did not evoke phase advances during early expiration (Alsahafi et
282 al., 2015). But in that experimental context a synapsin promoter drove channelrhodopsin
283 expression in both excitatory and inhibitory preBötC neurons. Because preBötC rhythmogenesis
284 depends on recurrent excitation, and the network is at the nadir of its excitability during early
285 expiration (Del Negro et al., 2018; Feldman and Kam, 2015; Ramirez et al., 2016),

286 photostimulation of inhibitory neurons in concert with excitatory neurons would be less effective
287 to evoke inspiratory bursts during early expiration.

288 Selective photostimulation of excitatory Dbx1-derived preBötC neurons should evoke phase
289 advances during early expiration, and it does. Cui *et al*. (2016) photostimulated excitatory Dbx1
290 neurons and evoked phase advances of up to ~72º during most of expiratory phase, except
291 during the inspiratory-expiratory transition. We evoked more substantial phase advances of 90-
292 150º during the early expiration. These results are not in conflict, but key methodological
293 differences may explain the discrepancy. Cui *et al*. anesthetized their mice and applied a
294 maximum laser power of 7 mW to activate channelrhodopsin, whereas we used awake or lightly
295 sedated mice and applied a maximum laser power of 10.2 mW to activate the channelrhodopsin
296 variant CatCh. Assuming that the fiberoptic appliances in both studies equally attenuate laser
297 power from box to preBötC, then the larger phase advances we evoked during early expiration
298 could be attributable to a higher excitability level of the preBötC in the unanesthetized (or lightly
299 sedated) mice, higher laser power, as well as the accelerated response time, enhanced light
300 sensitivity, and larger voltage responses evoked by photoactivated CatCh compared to ChR2
301 (Kleinlogel et al., 2011).

302 Brief photoinhibition of Dbx1 preBötC neurons during inspiration shortened it (i.e., decreased T_i)
303 and initiated the next cycle earlier than expected, a phase advance. We infer that
304 hyperpolarizing rhythmogenic neurons checks the recurrent excitation process, which impedes
305 but does not prevent inspiration. Nevertheless, the evoked breath is shorter in duration. preBötC
306 neurons do not overexcite or become refractory, which facilitates the onset of the next cycle,
307 hence the phase advance. That mechanism, here evoked by ArchT, mirrors the role of
308 endogenous phasic synaptic inhibition, which curbs recurrent excitation to limiting inspiratory
309 activity and facilitate inspiratory-expiratory phase transition (Baertsch et al., 2018). We found
310 that photoinhibition during expiration consistently caused a phase delay, which indicates
311 hyperpolarization of Dbx1 preBötC neurons resets recurrent excitation and thus prolongs the
312 interval until the next inspiration.

313 Our interpretations of the phase-response experiments, both photostimulation and
314 photoinhibition, are consistent with Dbx1 preBötC neurons having direct temporal control over
315 inspiration as well as post-inspiration and the expiratory interval. That conclusion may seem
316 overly broad considering, first, that the preBötC is the acknowledged inspiratory oscillator and,
317 second, that oscillator microcircuits for post-inspiration (the postinspiratory complex, PiCo,

Anderson et al., 2016) and expiration (the lateral parafacial group, $pF_{L,}$ Huckstepp et al., 2016, 2015; Pagliardini et al., 2011) also exist. Nevertheless, the preBötC plays a dominant role in organizing all phases of breathing by entraining the other oscillators in intact mice, and in reduced preparations that retain PiCo and pF_L (Del Negro et al., 2018; Moore et al., 2013; Ramirez et al., 2016). Therefore, the present data are consistent with Dbx1 preBötC interneurons constituting the oscillator core for inspiration and the central organizer for breathing.

Could optogenetic perturbation of inputs to the preBötC modulate breathing?

The intersectional mouse genetics in Dbx1;ArchT mice leads to fusion protein expression in Dbx1-derived cells throughout the neuraxis. Therefore, preBötC illumination inhibits constituent interneurons but also axons of passage and the axon terminals of Dbx1 neurons from remote locations (Ruangkittisakul et al., 2014) that could disfacilitate the preBötC. If disfacilitation were primarily modulating preBötC activity in Dbx1;ArchT mice, then light-evoked hyperpolarization should be commensurate in non-Dbx1 neurons (which do not express ArchT) and Dbx1 neurons; and, TTX should block it in both cases. However, non-Dbx1 neurons hyperpolarized ~1 mV in response to maximum illumination whereas Dbx1 neurons hyperpolarized ~11 mV, and TTX did not notably affect either response. We conclude that direct postsynaptic hyperpolarization of Dbx1 preBötC neurons, rather than a reduction of tonic excitatory drive, is the predominant effect of preBötC illumination in Dbx1;ArchT mice.

Light-evoked breathing changes in Dbx1;CatCh mice cannot be explained by photostimulation of axon terminals and axons of passage that originate outside of, but synapse within, the preBötC. We used double-stop technology to limit CatCh expression to Dbx1-derived neurons (not glia, see below), whose somas reside in the preBötC or directly adjacent sites including the Bötzinger complex of inhibitory neurons (Ezure et al., 2003; Tanaka et al., 2003), and the rostral ventral respiratory group (Dobbins and Feldman, 1994; Ellenberger and Feldman, 1990; Gaytán et al., 2002) of excitatory phrenic premotor neurons. If Dbx1-derived expiratory neurons in the Bötzinger complex exist (which has not been demonstrated), then their photostimulation would depress breathing (Janczewski et al., 2013; Marchenko et al., 2016), the opposite of what we measured. If photostimulation affected Dbx1 phrenic premotor neurons in the rostral ventral respiratory group (Wu et al., 2017), then that would enhance the magnitude of inspiratory breaths, but not the inspiratory timing circuits in the preBötC. Sustained photostimulation experiments only enhanced breathing frequency and never V_T, which diminishes the likelihood

that our protocols influenced Dbx1-derived phrenic premotoneurons. Thus, this caveat is unlikely to affect our primary conclusions regarding rhythmogenesis.

Effects on Dbx1-derived glia in the preBötC

Dbx1-expressing precursor cells develop into neurons and glia (Bouvier et al., 2010; Gray et al., 2010; Kottick et al., 2017; Ruangkittisakul et al., 2014) but optogenetic perturbation of glia is unlikely to have influenced the present results. First, we consider photoinhibition. Astrocytes support excitatory synaptic function in the preBötC (Hülsmann et al., 2000), but that role is metabolic in nature and light-evoked hyperpolarization would not preclude it. Calcium excitability and gliotransmission, which could be affected by photoinhibition, pertain to purinergic modulation and hypoxic challenges to the preBötC (Angelova et al., 2015; Funk et al., 2015; Huxtable et al., 2010; Rajani et al., 2017), but are less relevant factors governing the basal breathing state, which is the baseline for our experiments.

Photostimulation experiments unambiguously identify neurons as the cellular population that forms the core inspiratory oscillator. CatCh expression was induced following Cre/Lox and Frt/Flp recombination. We used a synapsin promoter to express Flp locally in the preBötC so only Dbx1 neurons would be transfected and express CatCh.

ArchT expression is selectively (but not exclusively) limited to neurons by the timing of tamoxifen administration. Inducing Cre/lox recombination in pregnant *Dbx1*^{CreERT2} mice at E9.5 reduces ArchT expression in glia to ~40%, whereas ArchT expression in neurons remains above 90% (Kottick et al., 2017), which increases our confidence that photoinhibition largely affects neurons (not glia) and that neurons are the predominate rhythmogenic constituents and most parsimonious explanation for the light-induced changes in breathing.

Size of the Dbx1 core oscillator

Up to 73% of Dbx1 preBötC neurons serve non-rhythmogenic functions: 56% influence arousal (Yackle et al., 2017) and 17% influence motor pattern (Cui et al., 2016), which accounts nearly three-quarters of the Dbx1 population in the preBötC. What implications does that have for the composition and size of the inspiratory core oscillator whose constituent interneurons are Dbx1-derived too?

Dbx1-Cdh9 preBötC neurons were certainly photoinhibited and photostimulated in our experiments. However, those neurons influence behavioral state (e.g., eupnea, grooming, exploring, sniffing, etc.) rather than cycle-to-cycle breathing dynamics. We applied optogenetic

perturbations only during eupnea, not during grooming or active movement, to control for behavioral shifts. Given that Dbx1-Cdh9 neurons are either weakly or not rhythmic (Yackle et al., 2017), briefly perturbing them would not influence the phase-response relationships, and thus would not confound our interpretation that Dbx1 preBötC neurons (even if a limited fraction of them) comprise the core oscillator.

Illumination of Sst-expressing Dbx1 neurons could be responsible for the decreases in V_T and apneas we report during sustained photoinhibition. In general, perturbations of Sst-expressing preBötC neurons affect breathing motor pattern in vagotomized and non-vagotomized adult mice (Cui et al., 2016; Koizumi et al., 2016); those effects are strong enough to completely stop breathing movements in intact adult rats (Tan et al., 2008). Our experiments would only impact neurons that are both Dbx1-dervied and Sst-expressing, thus a smaller population than Tan *et al.* (2008) manipulated. Nevertheless, to the extent that photoinhibition decreased breath magntidue and caused apnea, we attribute in part to direct effects on pattern-related Sst-expressing Dbx1-derived preBötC neurons that are either premotor part of a larger pattern-generating system (Cui et al., 2016; Revill et al., 2015; Wu et al., 2017).

If Cdh9 and Sst subpopulations of Dbx1 preBötC neurons are independent of the core respiratory oscillator, then only a small fraction (~27%) of Dbx1 neurons are available for rhythmogenesis. Dbx1 neurons that comprise the preBötC core number approximately 600 (Kottick et al., 2017; Wang et al., 2014). If one excludes Cdh9 and Sst neurons from this estimation, then as few as 160 Dbx1 preBötC neurons would remain for rhythmogenesis (we assue subpopulations serve one function). Can such a small number of interneurons comprise the inspiratory core oscillator?

Holographic photolysis of caged glutamate onto 4-9 preBötC neurons evokes inspiratory motor output *in vitro* (Kam et al., 2013). This type of stimulation would affect Dbx1-Cdh9 neurons that are weakly or non-rhythmic (Kam et al., 2013; Yackle et al., 2017) as well as inhibitory preBötC neurons (Kuwana et al., 2006; Morgado-Valle et al., 2010; Winter et al., 2009) so it may overestimate the minimum number of activated preBötC neurons needed to evoke inspiratory bursts. Regardless, a reasonable conclusion is that stimulating relatively small numbers of preBötC neurons are capable of inducing inspiratory burst cycles, which lends credence to the notion that a small subfraction of Dbx1 preBötC neurons could be rhythmogenic in the midst of a potentially larger population of non-rhythmogenic (both pattern-generating and non-respiratory) preBötC neurons.

Glutamatergic preBötC neurons not derived from Dbx1-expressing precursors may also comprise part of the core oscillator (Baertsch et al., 2018; Koizumi et al., 2016). We cannot precisely estimate the size of that subpopulation but we expect that it will be small based on the small fraction of preBötC neurons that express Vglut2 but not Dbx1 (Bouvier et al., 2010; Gray et al., 2010).

Dbx1 core hypothesis

The rhythmogenic subset of Dbx1 preBötC interneurons may be small, perhaps as little as 27% of the total Dbx1 population, but their outsize contribution to rhythmogenesis is unmistakable given the robust effects of sustained and transient photoinhibition and photostimulation demonstrated here, and by prior reports (Alsahafi et al., 2015; Cui et al., 2016; Koizumi et al., 2016). Therefore, whatever else Dbx1 preBötC neurons do – influence motor pattern and behavioral state – they certainly comprise the inspiratory core oscillator. Two key challenges going forward will be, first, to quantify the proportion of the rhythmogenic preBötC core that is non-Dbx1-derived, and second, to discriminate either on the basis of genetic or other markers, rhythmogenic from non-rhythmogenic Dbx1 neurons.

MATERIALS AND METHODS

Mice

The Institutional Animal Care and Use Committee at The College of William and Mary approved these protocols. Female mice that express tamoxifen-sensitive Cre recombinase in *Dbx1*-derived progenitor cells, i.e., *Dbx1*^{CreERT2} (Ruangkittisakul et al., 2014), available at Jax (strain 028131, Jackson Laboratories, Bar Harbor, ME, USA), were mated with males from two different reporter strains. The first reporter strain expresses an Archaerhodopsin-3 tagged with EGFP fusion protein (ArchT-EGFP) in a Cre-dependent manner from the endogenous *Gt(ROSA)26Sor* locus (Allen Institute nomenclature, Ai40D; Jax strain #021188,). The second reporter strain features *Frt*- and *LoxP*-flanked STOP cassettes followed by a fusion gene coding for calcium translocating channelrhodopsin and EYFP (CatCh-EYFP), which is expressed following Cre- and Flp-mediated recombination (Allen Institute nomenclature, Ai80D; Jax strain #025109). We administered tamoxifen to pregnant dams (22.5 mg/kg) at embryonic day 9.5 to maximize neuronal expression and minimize glial expression (Kottick et al., 2017). Dbx1;ArchT or Dbx1;CatCh mice were distinguished from wildtype (WT) littermates, which lack EGFP or

443 EYFP, via post-hoc histology. Therefore, WT littermates formed a control group whose
444 constituent members were unknown to the experimenter.

445 ***Brainstem slices***

446 Neonatal Dbx1;ArchT mice (0-4 days old) were anesthetized via hypothermia, decerebrated,
447 and then dissected in 4º C artificial cerebrospinal fluid (aCSF) containing (in mM): 124 NaCl, 3
448 KCl, 1.5 $CaCl_2$, 1 $MgSO_4$, 25 $NaHCO_3$, 0.5 NaH_2PO_4, and 30 dextrose aerated continually with
449 carbogen (95% O_2 and 5% CO_2) at pH 7.4. The isolated neuraxes were glued to an agar block
450 and mounted rostral side up in the vise of a vibratome. We cut the neuraxes in the transverse
451 plane to obtain a single 500-µm-thick section containing the preBötC as well as the hypoglossal
452 (XII) cranial motor nucleus and its rostral nerve rootlets. The anatomical criteria for isolating the
453 preBötC in rhythmically active slices from neonatal Dbx1-reporter mice are detailed in a series
454 of open access atlases (Ruangkittisakul et al., 2014). Slices were anchored using a silver wire
455 grid in a recording chamber on a fixed-stage upright physiology microscope. We perfused the
456 slice with aCSF at 27º C (2 ml/min) and elevated the K^+ concentration to 9 mM. Inspiratory
457 motor output was recorded from the XII nerve rootlets using a differential amplifier (gain 2000x)
458 and a band-pass filter (300-1000 Hz). Nerve root output was full-wave rectified and smoothed
459 for display.

460 We identified Dbx1 neurons under epifluorescence via EGFP expression and then performed
461 whole-cell patch-clamp recordings under visual control. Patch pipettes with tip resistance of 4-6
462 MΩ were fabricated from capillary glass (1.50 mm outer diameter, 0.86 mm inner diameter) and
463 filled with solution containing (in mM): 140 potassium gluconate, 5 NaCl, 0.1 EGTA, 10 HEPES,
464 2 Mg-ATP, and 0.3 Na_3-GTP. Alexa 568 hydrazide dye was added to the patch-pipette solution
465 (50 µM, Invitrogen, Carlsbad, CA, USA) as a color contrast to EGFP following whole-cell
466 dialysis. Membrane potential was amplified (100x) and low-pass filtered (1 kHz) using a patch-
467 clamp amplifier (EPC10, HEKA Elektronic, Holliston, MA, USA) and digitally acquired at 4 kHz
468 (PowerLab 4/30, AD Instruments, Colorado Springs, CO, USA).

469 ***Virus injection and fiber optic implantation***

470 We anesthetized adult Dbx1;ArchT and Dbx1;CatCh (aged 8-20 weeks) mice via intraperitoneal
471 injection of ketamine (100 mg/kg) and xylazine (10 mg/kg) and performed aseptic surgeries in
472 the prone position using a stereotaxic frame. After exposing the skull, we performed either one

(Dbx1;CatCh mice) or two (Dbx1;ArchT mice) 0.5-mm-diameter craniotomies in the range 6.95 to 7.07 mm posterior to bregma and 1.1 to 1.3 mm lateral to the midline suture.

In Dbx1;CatCh mice, we unilaterally injected an adeno-associated virus (AAV) immediately prior to fiber optic implantation to induce Flp-mediated recombination. We loaded an ultrafine, microvolume syringe (Neuros series, Hamilton, Reno, NV) with 120 µl of AAV-eSyn-FLPo (titer 10^{13} vg/ml, Vector Biolabs, Malvern, PA, USA). The syringe was lowered at 10 µm/s through the cerebellum and the virus was injected at the target site at approximately 60 nl/min. The syringe remained in place for 10 min before being retracted at 10 µm/s.

Both Dbx1;ArchT and Dbx1;CatCh mice were equipped with fiber optic appliances constructed by joining 1.27-mm-diameter ceramic ferrules (Precision Fiber Products, Milptas, CA, USA) with 105-µm-diameter 0.22 numerical aperture (NA) multimode fibers (Thorlabs, Newton, NJ, USA). We implanted fiber optic appliances bilaterally in Dbx1;ArchT mice and unilaterally in Dbx1;CatCh mice at a depth of 5.5 to 5.9 mm from bregma, which were secured with a cyanoacrylate adhesive (Loctite 3092, Henkel Corp., Rocky Hill, CT, USA). Dbx1;ArchT animals recovered for a minimum of 10 days before any further experimentation. Dbx1;CatCh mice recovered for a minimum of 21 days before further experimentation.

Breathing measurements

After anesthetizing mice using 2% isoflurane we connected the ferrules of Dbx1;ArchT mice to a 589-nm laser (Dragon Lasers, Changchun, China). The ferrule of Dbx1;CatCh mice was connected to a 473-nm laser (Dragon Lasers). Mice recovered from isofluorane anesthesia for ~1 hr, and then we measured breathing behavior using a whole body plethysmograph (Emka Technologies, Falls Church, VA, USA) that allowed for fiberoptic illumination in a sealed chamber.

In a separate session, these same mice were lightly sedated via intraperitoneal ketamine injections (15 mg/kg minimum dose), which we titrated as needed to reduce limb movements but retain toe-pinch and blink reflexes. The maximum aggregate dose was limited to 50 mg/kg. Mice were fitted with a modified anesthesia mask (Kent Scientific, Torrington, CT, USA) to measure breathing.

We applied a circuit of positive pressure, with balanced vacuum, to continuously flush the plethysmograph with breathing air. The plethysmograph and the mask were connected to a 1-

liter respiratory flow head and differential pressure transducer that measured airflow; positive airflow reflects inspiration in all cases. Analog breathing signals were digitized at 1 kHz (PowerLab).

Optogenetic protocols

We applied 5 s bouts of light (either 473 or 589 nm) to Dbx1;ArchT and Dbx1;CatCh mice at graded intensities of 6.8, 8.6, and 10.2 mW. All ferrules were tested with a power meter prior to implantation to verify that illumination intensity did not vary more than 0.1 mW from the specified values. Bouts of light application were separated by a minimum interval of 30 s. We also applied 100 ms light pulses at a fixed intensity of 10.2 mW. We exposed each mouse to 85-200 pulses spaced at random intervals of between 1 and 5 s.

We applied 2 s bouts of 589-nm light (at the same intensities listed above) to rhythmically active slices. The fiberoptics were targeted to selectively illuminate the preBötC bilaterally but not the adjacent reticular formation.

Data analyses

The airflow signal was band-pass filtered (0.1-20 Hz) and analyzed using LabChart 8 software (AD Instruments), which computes airflow (units of ml/s), respiratory rate (i.e., frequency, f, units of Hz), tidal volume (V_T, units of ml), inspiratory time (T_i), and minute ventilation (MV, units of ml/min). We computed statistics using GraphPad Prism 6 (La Jolla, CA, USA) and R: The Project for Statistical Computing (R, The R Foundation, Vienna, Austria) and prepared figures using Adobe Illustrator (Adobe Systems Inc., San Jose, CA, USA), GraphPad Prism 6, and IGOR Pro 6 (Wavemetrics, Lake Oswego, OR, USA). We analyzed the experiments in which 5 s light pulses were applied to the preBötC using paired t-tests, specifically comparing mean f, V_T, and MV for control and illumination conditions at three different light intensity levels (i.e., at each laser strength tested, the pre-illumination ventilation serves as its own control).

We analyzed phase-response relationships of the breathing cycles perturbed by 100 ms-duration light pulses (see Figure 3C inset). The expected cycle period was measured from the unperturbed cycle immediately before the light pulse, which was defined as spanning 0-360º ($\Phi_{Expected}$). Cycle times were measured from the start of inspiration in one breath to the start of inspiration of the subsequent breath. For perturbed cycles, 100-ms light pulses were applied at random time points spanning the inspiration and expiration to test for phase shifts. Φ_{Stim} marks

the phase at which the light pulse occurred. The induced cycle period ($\Phi_{Induced}$) was measured from the perturbed cycle. The perturbation of breathing phase, Φ_{Shift}, was defined as the difference between $\Phi_{Induced}$ and $\Phi_{Expected}$. We calculated change in V_T and T_i in the perturbed breath compared to the expected breath normalized to the expected breath (refered to as, ΔV_T and ΔT_i, respectively). Further, we calculated the phase shift of the breath following the perturbed breath (i.e., the cycle after $\Phi_{Induced}$) also with respect to $\Phi_{Expected}$; we refer to the phase of the subsequent breath Φ_{N+1}. Measurements of Φ_{Shift}, ΔV_T, ΔT_i, and Φ_{N+1} are all linked to a particular Φ_{Stim} within the interval 0-360º. To analyze group data we sorted Φ_{Stim} into 12 equally sized 30º bins. We computed the mean and standard deviation (SD) for Φ_{Shift}, ΔV_T, ΔT_i, and Φ_{N+1} within each bin, which we then plotted in phase-response curves along with values calculated from wild type littermates. A Tukey's HSD to test was used to evaluate how unlikely it would have been to obtain mean Φ_{Shift}, ΔV_T, ΔT_i, and Φ_{N+1} for each bin if the optogenetic perturbations had commensurate effects on Dbx1;ArchT (or Dbx1;CatCh) mice and wild type littermates.

Histology

After experimentation we verified in all animals that fiber optic tips were within 500 µm of the dorsal preBötC border, which could be identified via well-established anatomical criteria in combination with either ArchT-EGFP or CatCh-EYFP fusion protein expression in reporter mice (Figure 1C). We administered a lethal dose of pentobarbital (100 mg/kg i.p.) and then transcardially perfused the mice with 1x PBS followed by 4% PFA in PBS. The neuraxes were removed and post-fixed overnight in 4% PFA, and later sliced in 50-µm contiguous transverse sections using a vibratome. Free-floating sections were stained using NeuroTrace 530/615 red fluorescent nissl stain (Invitrogen) for 1 hr, rinsed in PBSand then cover-slipped using Vectashield (Vector Labs, Burlingame, CA, USA). Tissue sections were visualized using bright-field and confocal microscopy. Images were arranged as mosaics and brightness and contrast were adjusted uniformly across the entire ensemble image using the public domain software package ImageJ. Images were not manipulated in any other way.

REFERENCES

Alsahafi, Z., Dickson, C.T., and Pagliardini, S. (2015). Optogenetic excitation of preBötzinger complex neurons potently drives inspiratory activity in vivo. J. Physiol. n/a-n/a.

Anderson, T.M., Garcia, A.J., Baertsch, N.A., Pollak, J., Bloom, J.C., Wei, A.D., Rai, K.G., and Ramirez, J.-M. (2016). A novel excitatory network for the control of breathing. Nature *536*, 76–80.

565 Angelova, P.R., Kasymov, V., Christie, I., Sheikhbahaei, S., Turovsky, E., Marina, N., Korsak,
566 A., Zwicker, J., Teschemacher, A.G., Ackland, G.L., et al. (2015). Functional Oxygen Sensitivity
567 of Astrocytes. J. Neurosci. Off. J. Soc. Neurosci. *35*, 10460–10473.

568 Baertsch, N.A., Baertsch, H., and Ramirez, J.M. (2018). The interdependence of excitation and
569 inhibition for the control of dynamic breathing rhythms. Press.

570 Bouvier, J., Thoby-Brisson, M., Renier, N., Dubreuil, V., Ericson, J., Champagnat, J., Pierani, A.,
571 Chédotal, A., and Fortin, G. (2010). Hindbrain interneurons and axon guidance signaling critical
572 for breathing. Nat. Neurosci. *13*, 1066–1074.

573 Cui, Y., Kam, K., Sherman, D., Janczewski, W.A., Zheng, Y., and Feldman, J.L. (2016). Defining
574 preBötzinger Complex Rhythm- and Pattern-Generating Neural Microcircuits In Vivo. Neuron
575 *91*, 602–614.

576 Del Negro, C.A., Funk, G.D., and Feldman, J.L. (2018). Breathing matters. Nat Rev Neurosci.

577 Dobbins, E.G., and Feldman, J.L. (1994). Brainstem network controlling descending drive to
578 phrenic motoneurons in rat. J. Comp. Neurol. *347*, 64–86.

579 Dutschmann, M., Jones, S.E., Subramanian, H.H., Stanic, D., and Bautista, T.G. (2014).
580 Chapter 7 - The physiological significance of postinspiration in respiratory control. In Progress in
581 Brain Research, G. Holstege, C.M. Beers, and H.H. Subramanian, eds. (Elsevier), pp. 113–130.

582 Ellenberger, H.H., and Feldman, J.L. (1990). Brainstem connections of the rostral ventral
583 respiratory group of the rat. Brain Res. *513*, 35–42.

584 Ezure, K., Tanaka, I., and Saito, Y. (2003). Brainstem and spinal projections of augmenting
585 expiratory neurons in the rat. Neurosci. Res. *45*, 41–51.

586 Feldman, J.L., and Del Negro, C.A. (2006). Looking for inspiration: new perspectives on
587 respiratory rhythm. Nat. Rev. Neurosci. *7*, 232–242.

588 Feldman, J.L., and Kam, K. (2015). Facing the challenge of mammalian neural microcircuits:
589 taking a few breaths may help. J. Physiol. *593*, 3–23.

590 Feldman, J.L., Negro, C.A.D., and Gray, P.A. (2013). Understanding the Rhythm of Breathing:
591 So Near, Yet So Far. Annu. Rev. Physiol. *75*, 423–452.

592 Funk, G.D., and Greer, J.J. (2013). The rhythmic, transverse medullary slice preparation in
593 respiratory neurobiology: Contributions and caveats. Respir. Physiol. Neurobiol. *186*, 236–253.

594 Funk, G.D., Smith, J.C., and Feldman, J.L. (1993). Generation and transmission of respiratory
595 oscillations in medullary slices: role of excitatory amino acids. J Neurophysiol *70*, 1497–1515.

596 Funk, G.D., Rajani, V., Alvares, T.S., Revill, A.L., Zhang, Y., Chu, N.Y., Biancardi, V., Linhares-
597 Taxini, C., Katzell, A., and Reklow, R. (2015). Neuroglia and their roles in central respiratory
598 control; an overview. Comp. Biochem. Physiol. A. Mol. Integr. Physiol. *186*, 83–95.

599 Gaytán, S.P., Pásaro, R., Coulon, P., Bevengut, M., and Hilaire, G. (2002). Identification of
600 central nervous system neurons innervating the respiratory muscles of the mouse: a
601 transneuronal tracing study. Brain Res. Bull. *57*, 335–339.

602 Gray, P.A., Rekling, J.C., Bocchiaro, C.M., and Feldman, J.L. (1999). Modulation of respiratory
603 frequency by peptidergic input to rhythmogenic neurons in the preBotzinger complex. Science
604 *286*, 1566–1568.

605 Gray, P.A., Janczewski, W.A., Mellen, N., McCrimmon, D.R., and Feldman, J.L. (2001). Normal
606 breathing requires preBotzinger complex neurokinin-1 receptor-expressing neurons. Nat
607 Neurosci *4*, 927–930.

608 Gray, P.A., Hayes, J.A., Ling, G.Y., Llona, I., Tupal, S., Picardo, M.C.D., Ross, S.E., Hirata, T.,
609 Corbin, J.G., Eugenín, J., et al. (2010). Developmental Origin of PreBötzinger Complex
610 Respiratory Neurons. J. Neurosci. *30*, 14883–14895.

611 Guerrier, C., Hayes, J.A., Fortin, G., and Holcman, D. (2015). Robust network oscillations during
612 mammalian respiratory rhythm generation driven by synaptic dynamics. Proc. Natl. Acad. Sci.
613 *112*, 9728–9733.

614 Huckstepp, R.T., Henderson, L.E., Cardoza, K.P., and Feldman, J.L. (2016). Interactions
615 between respiratory oscillators in adult rats. eLife *5*, e14203.

616 Huckstepp, R.T.R., Cardoza, K.P., Henderson, L.E., and Feldman, J.L. (2015). Role of
617 Parafacial Nuclei in Control of Breathing in Adult Rats. J. Neurosci. *35*, 1052–1067.

618 Hülsmann, S., Oku, Y., Zhang, W., and Richter, D.W. (2000). Metabolic coupling between glia
619 and neurons is necessary for maintaining respiratory activity in transverse medullary slices of
620 neonatal mouse. Eur. J. Neurosci. *12*, 856–862.

621 Huxtable, A.G., Zwicker, J.D., Alvares, T.S., Ruangkittisakul, A., Fang, X., Hahn, L.B., Chaves,
622 E.P. de, Baker, G.B., Ballanyi, K., and Funk, G.D. (2010). Glia Contribute to the Purinergic
623 Modulation of Inspiratory Rhythm-Generating Networks. J. Neurosci. *30*, 3947–3958.

624 Janczewski, W.A., Tashima, A., Hsu, P., Cui, Y., and Feldman, J.L. (2013). Role of Inhibition in
625 Respiratory Pattern Generation. J. Neurosci. *33*, 5454–5465.

626 Kam, K., Worrell, J.W., Ventalon, C., Emiliani, V., and Feldman, J.L. (2013). Emergence of
627 Population Bursts from Simultaneous Activation of Small Subsets of preBötzinger Complex
628 Inspiratory Neurons. J. Neurosci. *33*, 3332–3338.

629 Kleinlogel, S., Feldbauer, K., Dempski, R.E., Fotis, H., Wood, P.G., Bamann, C., and Bamberg,
630 E. (2011). Ultra light-sensitive and fast neuronal activation with the Ca^{2+}-permeable
631 channelrhodopsin CatCh. Nat. Neurosci. *14*, 513.

632 Koizumi, H., Mosher, B., Tariq, M.F., Zhang, R., Koshiya, N., and Smith, J.C. (2016). Voltage-
633 Dependent Rhythmogenic Property of Respiratory Pre-Bötzinger Complex Glutamatergic, Dbx1-
634 Derived, and Somatostatin-Expressing Neuron Populations Revealed by Graded Optogenetic
635 Inhibition. Eneuro *3*.

636 Kottick, A., and Del Negro, C.A. (2015). Synaptic Depression Influences Inspiratory-Expiratory
637 Phase Transition in Dbx1 Interneurons of the preBötzinger Complex in Neonatal Mice. J.
638 Neurosci. Off. J. Soc. Neurosci. *35*, 11606–11611.

639 Kottick, A., Martin, C.A., and Del Negro, C.A. (2017). Fate mapping neurons and glia derived
640 from Dbx1-expressing progenitors in mouse preBötzinger complex. Physiol. Rep. *5*, e13300.

641 Kuwana, S., Tsunekawa, N., Yanagawa, Y., Okada, Y., Kuribayashi, J., and Obata, K. (2006).
642 Electrophysiological and morphological characteristics of GABAergic respiratory neurons in the
643 mouse pre-Bötzinger complex. Eur. J. Neurosci. *23*, 667–674.

644 Marchenko, V., Koizumi, H., Mosher, B., Koshiya, N., Tariq, M.F., Bezdudnaya, T.G., Zhang, R.,
645 Molkov, Y.I., Rybak, I.A., and Smith, J.C. (2016). Perturbations of Respiratory Rhythm and
646 Pattern by Disrupting Synaptic Inhibition within Pre-Bötzinger and Bötzinger Complexes. eNeuro
647 ENEURO.0011-16.2016.

648 Moore, J.D., Deschênes, M., Furuta, T., Huber, D., Smear, M.C., Demers, M., and Kleinfeld, D.
649 (2013). Hierarchy of orofacial rhythms revealed through whisking and breathing. Nature *497*,
650 205–210.

651 Morgado-Valle, C., Baca, S.M., and Feldman, J.L. (2010). Glycinergic pacemaker neurons in
652 preBötzinger Complex of neonatal mouse. J. Neurosci. Off. J. Soc. Neurosci. *30*, 3634–3639.

653 Mutolo, D., Bongianni, F., Carfì, M., and Pantaleo, T. (2002). Respiratory changes induced by
654 kainic acid lesions in rostral ventral respiratory group of rabbits. Am. J. Physiol. - Regul. Integr.
655 Comp. Physiol. *283*, R227–R242.

656 Pagliardini, S., Janczewski, W.A., Tan, W., Dickson, C.T., Deisseroth, K., and Feldman, J.L.
657 (2011). Active Expiration Induced by Excitation of Ventral Medulla in Adult Anesthetized Rats. J.
658 Neurosci. *31*, 2895–2905.

659 Pantaleo, T., Mutolo, D., Cinelli, E., and Bongianni, F. (2011). Respiratory responses to
660 somatostatin microinjections into the Bötzinger complex and the pre-Bötzinger complex of the
661 rabbit. Neurosci. Lett. *498*, 26–30.

662 Picardo, M.C.D., Weragalaarachchi, K.T.H., Akins, V.T., and Del Negro, C.A. (2013).
663 Physiological and morphological properties of Dbx1-derived respiratory neurons in the pre-
664 Bötzinger complex of neonatal mice. J. Physiol. *591*, 2687–2703.

665 Rajani, V., Zhang, Y., Jalubula, V., Rancic, V., SheikhBahaei, S., Zwicker, J.D., Pagliardini, S.,
666 Dickson, C.T., Ballanyi, K., Kasparov, S., et al. (2017). Release of ATP by pre-Bötzinger
667 complex astrocytes contributes to the hypoxic ventilatory response via a Ca2+ -dependent
668 P2Y1 receptor mechanism. J. Physiol.

669 Ramirez, J.-M., Dashevskiy, T., Marlin, I.A., and Baertsch, N. (2016). Microcircuits in respiratory
670 rhythm generation: commonalities with other rhythm generating networks and evolutionary
671 perspectives. Curr. Opin. Neurobiol. *41*, 53–61.

672 Revill, A.L., Vann, N.C., Akins, V.T., Kottick, A., Gray, P.A., Negro, C.A.D., and Funk, G.D.
673 (2015). Dbx1 precursor cells are a source of inspiratory XII premotoneurons. eLife *4*, e12301.

674 Ruangkittisakul, A., Panaitescu, B., and Ballanyi, K. (2011). K+ and Ca2+ dependence of
675 inspiratory-related rhythm in novel “calibrated” mouse brainstem slices. Respir. Physiol.
676 Neurobiol. *175*, 37–48.

677 Ruangkittisakul, A., Kottick, A., Picardo, M.C.D., Ballanyi, K., and Del Negro, C.A. (2014).
678 Identification of the pre-Bötzinger complex inspiratory center in calibrated “sandwich” slices from
679 newborn mice with fluorescent Dbx1 interneurons. Physiol. Rep. *2*.

680 Schwarzacher, S.W., Smith, J.C., and Richter, D.W. (1995). Pre-Bötzinger complex in the cat. J.
681 Neurophysiol. *73*, 1452–1461.

682 Schwarzacher, S.W., Rüb, U., and Deller, T. (2010). Neuroanatomical characteristics of the
683 human pre-Bötzinger complex and its involvement in neurodegenerative brainstem diseases.
684 Brain awq327.

685 Smith, J.C., Ellenberger, H.H., Ballanyi, K., Richter, D.W., and Feldman, J.L. (1991). Pre-
686 Botzinger complex: a brainstem region that may generate respiratory rhythm in mammals.
687 Science *254*, 726–729.

688 Song, H., Hayes, J.A., Vann, N.C., Wang, X., LaMar, M.D., and Negro, C.A.D. (2016).
689 Functional Interactions between Mammalian Respiratory Rhythmogenic and Premotor Circuitry.
690 J. Neurosci. *36*, 7223–7233.

691 Stornetta, R.L., Rosin, D.L., Wang, H., Sevigny, C.P., Weston, M.C., and Guyenet, P.G.
692 (2003a). A group of glutamatergic interneurons expressing high levels of both neurokinin-1
693 receptors and somatostatin identifies the region of the pre-Bötzinger complex. J. Comp. Neurol.
694 *455*, 499–512.

695 Stornetta, R.L., Sevigny, C.P., and Guyenet, P.G. (2003b). Inspiratory augmenting bulbospinal
696 neurons express both glutamatergic and enkephalinergic phenotypes. J. Comp. Neurol. *455*,
697 113–124.

698 Tan, W., Janczewski, W.A., Yang, P., Shao, X.M., Callaway, E.M., and Feldman, J.L. (2008).
699 Silencing preBötzinger Complex somatostatin-expressing neurons induces persistent apnea in
700 awake rat. Nat. Neurosci. *11*, 538–540.

701 Tanaka, I., Ezure, K., and Kondo, M. (2003). Distribution of glycine transporter 2 mRNA-
702 containing neurons in relation to glutamic acid decarboxylase mRNA-containing neurons in rat
703 medulla. Neurosci. Res. *47*, 139–151.

704 Tupal, S., Rieger, M.A., Ling, G.-Y., Park, T.J., Dougherty, J.D., Goodchild, A.K., and Gray, P.A.
705 (2014). Testing the role of preBötzinger Complex somatostatin neurons in respiratory and vocal
706 behaviors. Eur. J. Neurosci. *40*, 3067–3077.

707 Vann, N.C., Pham, F.D., Hayes, J.A., Kottick, A., and Negro, C.A.D. (2016). Transient
708 Suppression of Dbx1 PreBötzinger Interneurons Disrupts Breathing in Adult Mice. PLOS ONE
709 *11*, e0162418.

710 Wallen-Mackenzie, A., Gezelius, H., Thoby-Brisson, M., Nygard, A., Enjin, A., Fujiyama, F.,
711 Fortin, G., and Kullander, K. (2006). Vesicular glutamate transporter 2 is required for central

712 respiratory rhythm generation but not for locomotor central pattern generation. J Neurosci *26*,
713 12294–12307.

714 Wang, X., Hayes, J.A., Revill, A.L., Song, H., Kottick, A., Vann, N.C., LaMar, M.D., Picardo,
715 M.C.D., Akins, V.T., Funk, G.D., et al. (2014). Laser ablation of Dbx1 neurons in the pre-
716 Bötzinger complex stops inspiratory rhythm and impairs output in neonatal mice. eLife *3*,
717 e03427.

718 Wenninger, J.M., Pan, L.G., Klum, L., Leekley, T., Bastastic, J., Hodges, M.R., Feroah, T.R.,
719 Davis, S., and Forster, H.V. (2004). Large lesions in the pre-Bötzinger complex area eliminate
720 eupneic respiratory rhythm in awake goats. J. Appl. Physiol. Bethesda Md 1985 *97*, 1629–1636.

721 Winter, S.M., Fresemann, J., Schnell, C., Oku, Y., Hirrlinger, J., and Hülsmann, S. (2009).
722 Glycinergic interneurons are functionally integrated into the inspiratory network of mouse
723 medullary slices. Pflugers Arch. *458*, 459–469.

724 Wu, J., Capelli, P., Bouvier, J., Goulding, M., Arber, S., and Fortin, G. (2017). A V0 core
725 neuronal circuit for inspiration. Nat. Commun. *8*, 544.

726 Yackle, K., Schwarz, L.A., Kam, K., Sorokin, J.M., Huguenard, J.R., Feldman, J.L., Luo, L., and
727 Krasnow, M.A. (2017). Breathing control center neurons that promote arousal in mice. Science
728 *355*, 1411–1415.

729

730

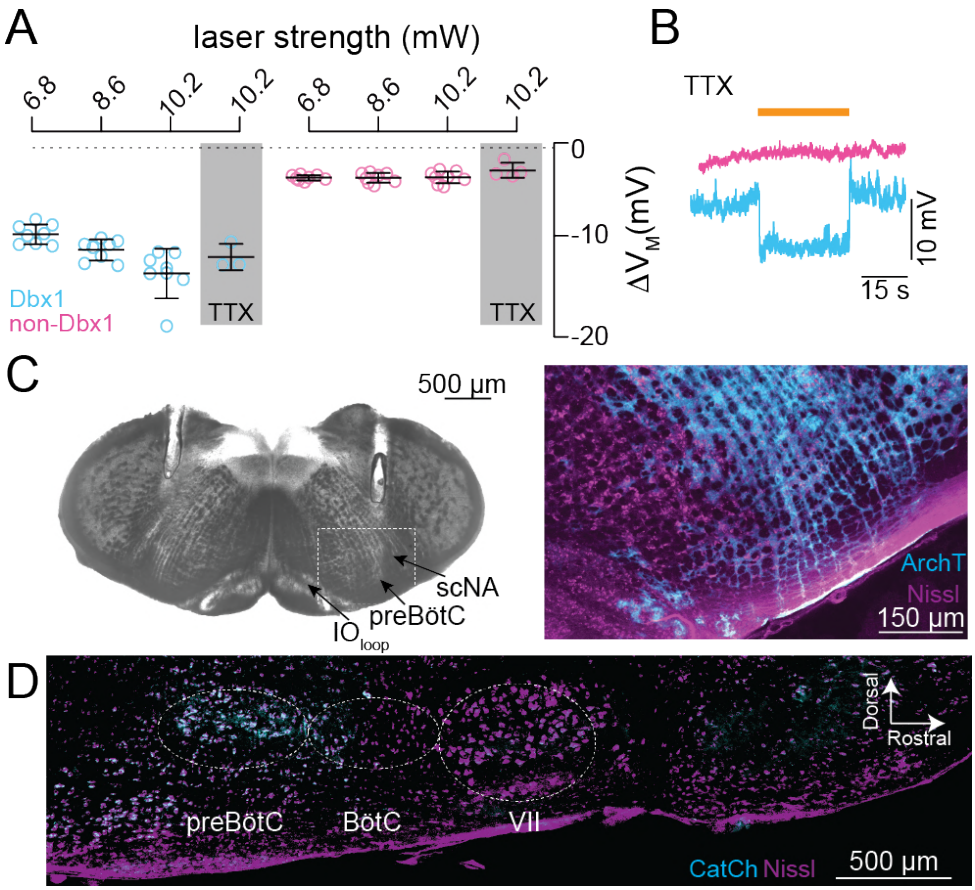

Figure 1. Photoinhibition of preBötC neurons *in vitro* and fusion protein expression patterns. **A**, Membrane hyperpolarization (ΔV_M) evoked by light pulses at three intensities in Dbx1 and non-Dbx1 preBötC neurons recorded from neonatal Dbx1;ArchT mouse slices. Bars show mean and SD (n = 8 Dbx1 neurons in control and n = 4 Dbx1 neurons in 1 µM tetrodotoxin [TTX]; n = 8 non-Dbx1 neurons in control and n = 4 non-Dbx1 neurons in TTX). **B**, Membrane trajectories in response to 30-s bouts of 10.2 mW illumination in 1 µM TTX. **C**, Bright field image of a transverse section from an adult Dbx1;ArchT mouse at the level the preBötC, as indicated by the loop of the inferior olive (IO_{loop}) and the semi-compact division of the nucleus ambiguus (scNA). Parallel tracks of implanted fiber optics are visible from the dorsal border of the tissue section into the intermediate reticular formation dorsal to the preBötC. The selection box was imaged using fluorescence microscopy to show ArchT (cyan) protein expression in the preBötC in detail, Nissl staining (magenta) included for contrast. **D**, Parasagittal section from an adult Dbx1;CatCh mouse. Nissl (magenta) shows anatomical landmarks including the facial (VII) cranial nucleus, Bötzinger complex (BötC), and the preBötC. CatCh (cyan) expression is limited to the preBötC.

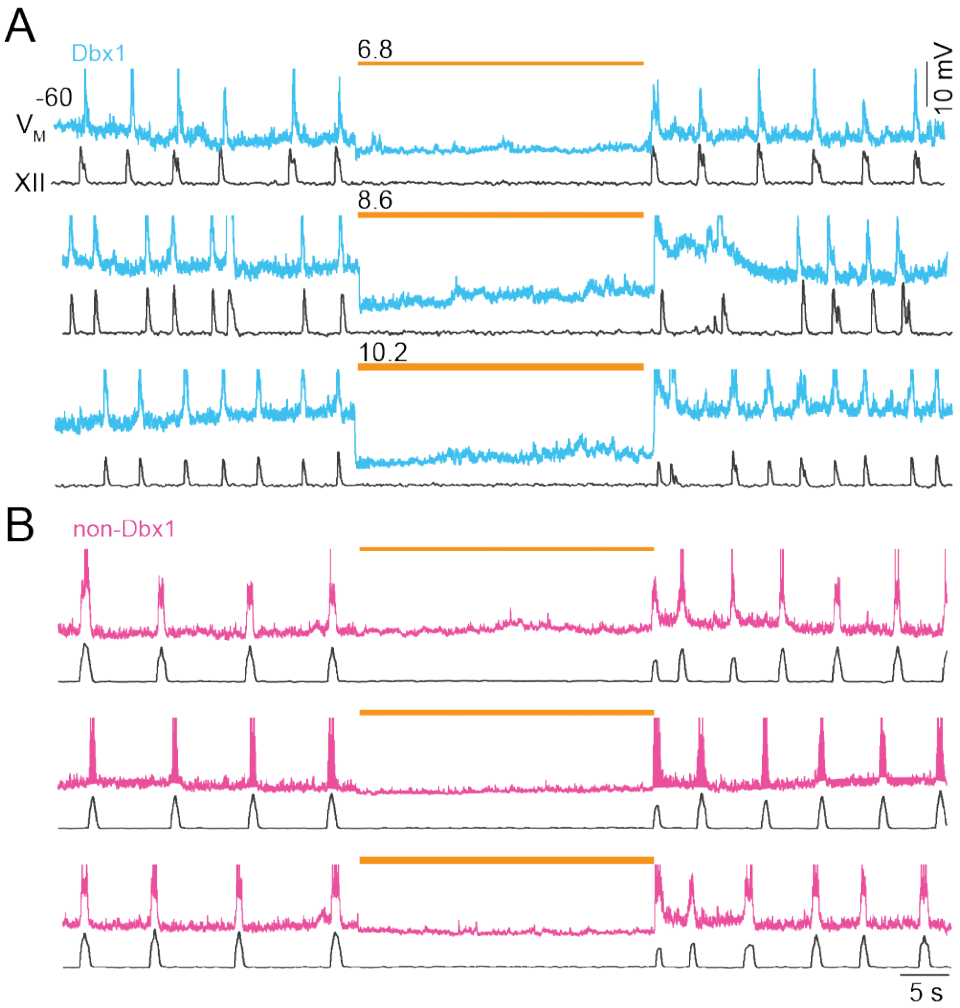

Figure 1 – figure supplement 1. Photoinhibition of preBötC neurons *in vitro*. **A**, Membrane trajectory of an ArchT-expressing Dbx1 preBötC neuron (V_M, cyan traces) in a rhythmically active slice preparation with inspiratory motor output recorded from the XII nerve rootlet. **B**, Membrane trajectory of a non-Dbx1, non-ArchT-expressing preBötC neuron (V_M, magenta traces) with XII motor output. Light pulses (30 s) were applied bilaterally to the preBötC at three intensities (units of mW) in A and B. Yellow line thickness corresponds to light intensity, which is also annotated above each line. Voltage and time calibrations apply to A and B, including baseline membrane potential of -60 mV. Action potentials have been truncated for display to emphasize the trajectory around the baseline membrane potential.

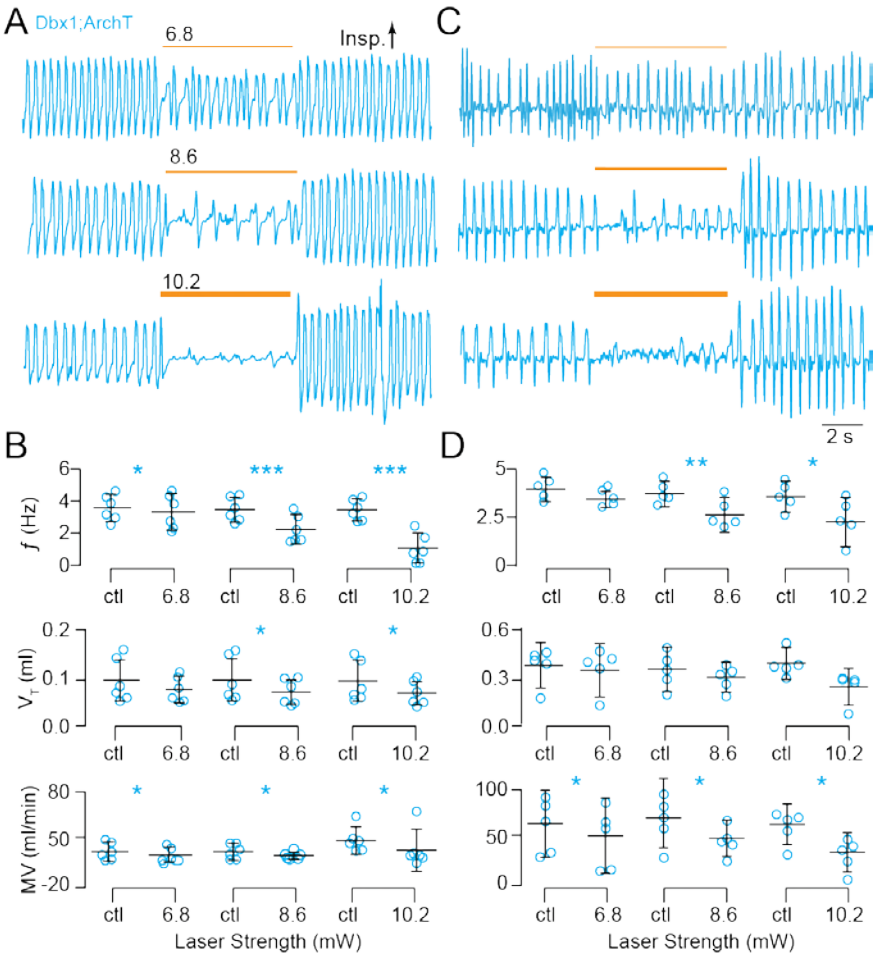

Figure 2. Photoinhibition of Dbx1 preBötC neurons depresses breathing in adult Dbx1;ArchT mice. **A**, Airflow traces from a sedated mouse exposed to 5-s bouts of bilateral preBötC illumination at three intensities (units of mW). Yellow line thickness corresponds to light intensity, which is also annotated above each line. **B**, Group data from experiments in A quantifying light-evoked changes in f, V_T and MV. Symbols show the mean f, V_T, and MV measured in each mouse. Bars show the mean and SD for all animals tested (n = 5). Control measurements are labeled 'ctl'; numerals indicate light intensity. **C**, Airflow traces from an awake unrestrained mouse exposed to 5-s bouts of bilateral preBötC illumination at three intensities. Yellow line thickness corresponds to light intensity; annotations mach those in A. **D**, Group data from experiments in C quantifying light-evoked changes in f, V_T and MV. Symbols show the mean f, V_T, and MV measured in each mouse. Bars show the mean and SD for all animals tested (n = 6). Control measurements are labeled 'ctl'; numerals indicate light intensity. Asterisks represent statistical significance at $p < 0.05$; the double asterisk represents $p < 0.01$; and triple asterisks represent $p < 0.001$.

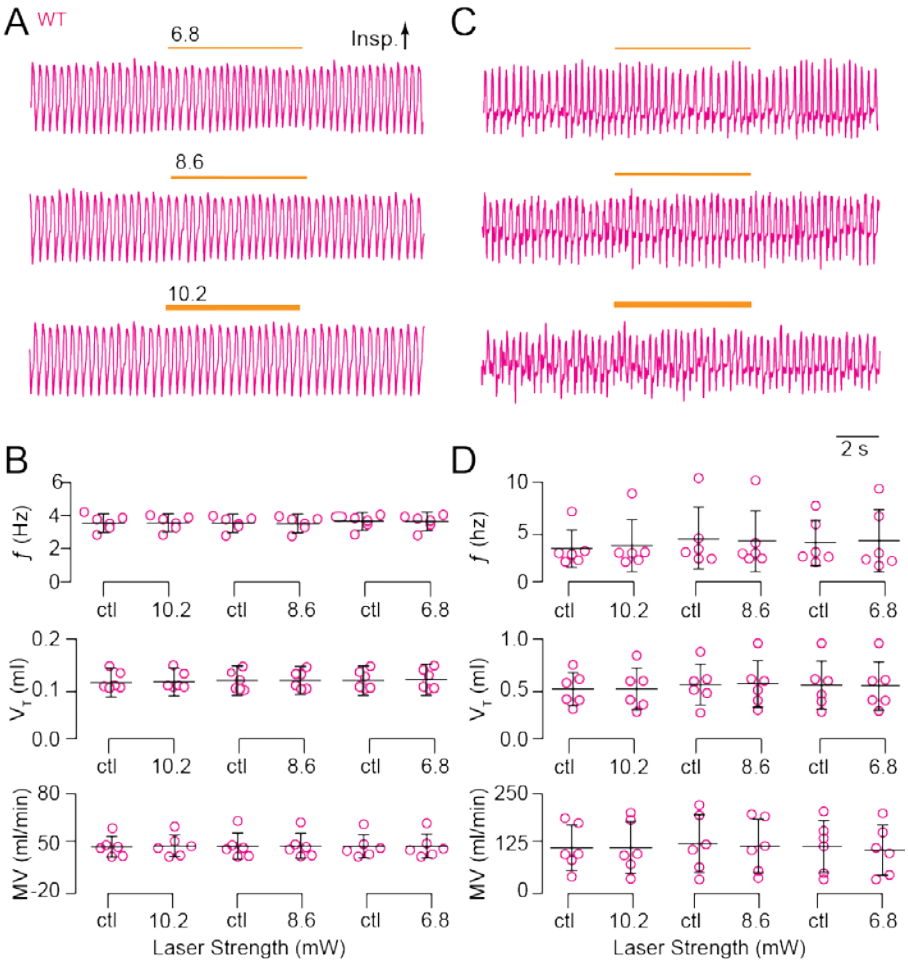

Figure 2 – figure supplement 1. Light application to the preBötC does not affect breathing in wild type Dbx1;ArchT littermates. **A**, Airflow traces from a sedated mouse exposed to 5-s bouts of bilateral preBötC illumination at three intensities (units of mW). Yellow line thickness corresponds to light intensity, which is also annotated above each line. **B**, Group data from experiments in A quantifying f, V_T and MV in response to light application. Symbols show mean f, V_T, and MV in each mouse. Bars show the mean and SD for all animals tested (n = 6). Control measurements are labeled 'ctl'; numerals indicate light intensity. **C**, Airflow traces from an awake unrestrained mouse exposed to 5-s bouts of unilateral preBötC illumination at three intensities (units of mW). Yellow line thickness corresponds to light intensity; annotations mach those in A. **D**, Group data from experiments in C quantifying f, V_T and MV in response to light application. Symbols show mean f, V_T, and MV in each mouse. Bars show the mean and SD for all animals tested (n = 6). Control measurements are labeled 'ctl'; numerals indicate light intensity.

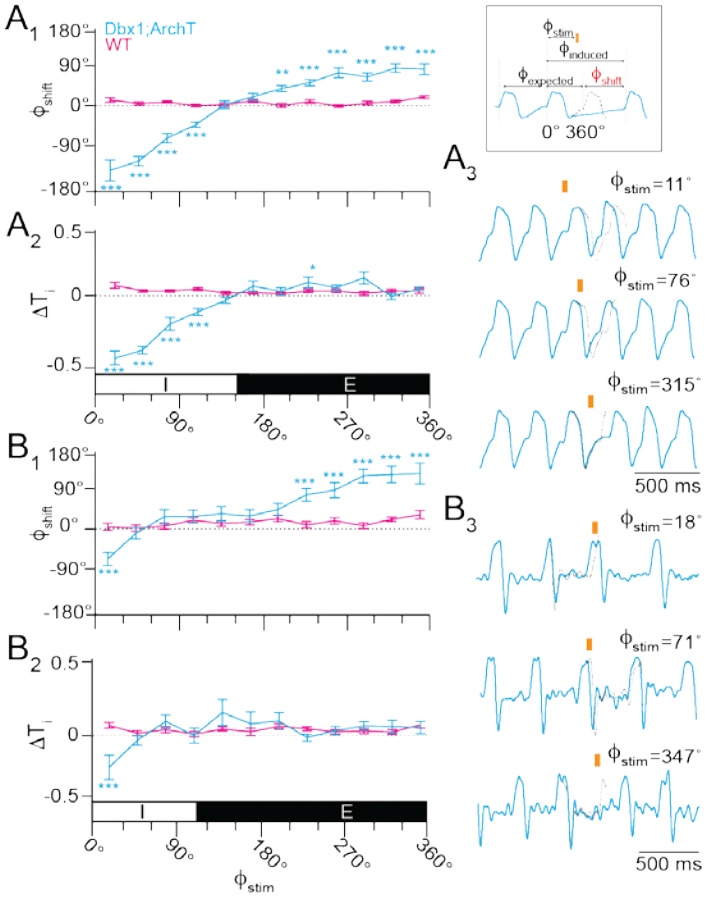

Figure 3. Effects of brief photoinhibition on the breathing phase and inspiratory duration in Dbx1;ArchT mice (n = 6 in A, n = 5 in B, cyan) and wild type littermates (n = 6, magenta). **A_1**, Phase-response curve plotting Φ_{Shift} following 100-ms photoinhibition at Φ_{Stim} throughout the breathing cycle in sedated mice. Φ_{Stim} was partitioned into 12 equally sized bins (30º) in A and B. **A_2**, Phase-response curve showing changes in T_i following brief photoinhibition (i.e., the perturbed breath) in the same cohort of sedated mice. The abscissa marks the inspiratory (I, 0-150º) and expiratory (E, 150-360º) phases of the breathing cycle (0-360º), which applies to A_1 and A_2. **A_3**, Sample airflow traces from a representative sedated mouse (Φ_{Stim} is indicated by an orange bar and numeral value). Time calibration is shown. **B_1**, Phase-response curve plotting Φ_{Shift} following brief photoinhibition at Φ_{Stim} throughout the breathing cycle in awake unrestrained mice. **B_2**, Phase-response curve showing changes in T_i following brief photoinhibition (i.e., the perturbed breath) in the same cohort of awake unrestrained mice. The abscissa marks the inspiratory (I, 0-110º) and expiratory (E, 110-360º) phases of the breathing cycle (0-360º), which applies to B_1 and B_2. **B_3**, Sample airflow traces from a representative awake unrestrained mouse (Φ_{Stim} is indicated by an orange bar and numeral value). Time calibration is shown.

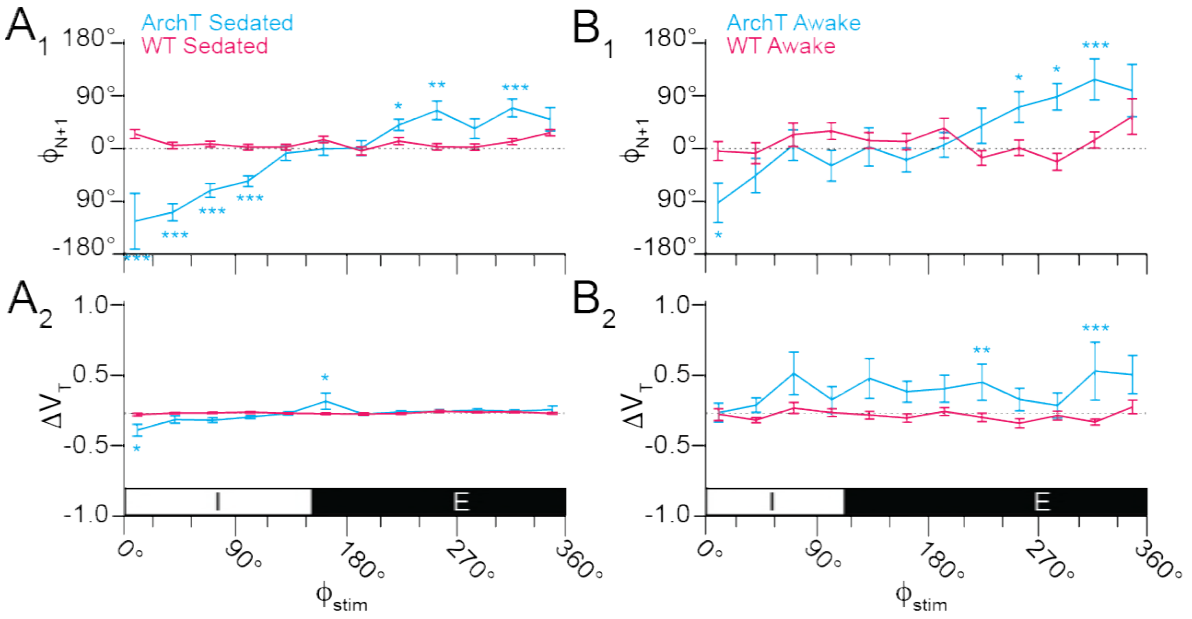

Figure 3 – figure supplement 1. Effects of brief photoinhibition on V_T and Φ_{N+1} in Dbx1;ArchT mice (n = 5 in A, n = 6 in B, cyan) and wild type littermates (n = 6, magenta). **A_1**, Phase-response curve plotting Φ_{N+1} vs. Φ_{Stim} throughout the breathing cycle in sedated mice. **A_2**, Phase-response curve for changes in V_T following brief photoinhibition (i.e., the perturbed breath) in the same cohort of sedated mice. The abscissa marks the inspiratory (I, 0-150º) and expiratory (E, 150-360º) phases of the breathing cycle (0-360º), which applies to A_1 and A_2. **B_1**, Phase-response curve plotting Φ_{N+1} vs. Φ_{Stim} in awake unrestrained mice. **B_2**, Phase-response curve for ΔV_T vs. Φ_{Stim} in the same cohort of awake unrestrained mice. The abscissa marks the inspiratory (I, 0-110º) and expiratory (E, 110-360º) phases of the complete breathing cycle (0-360º), which applies to B_1 and B_2.

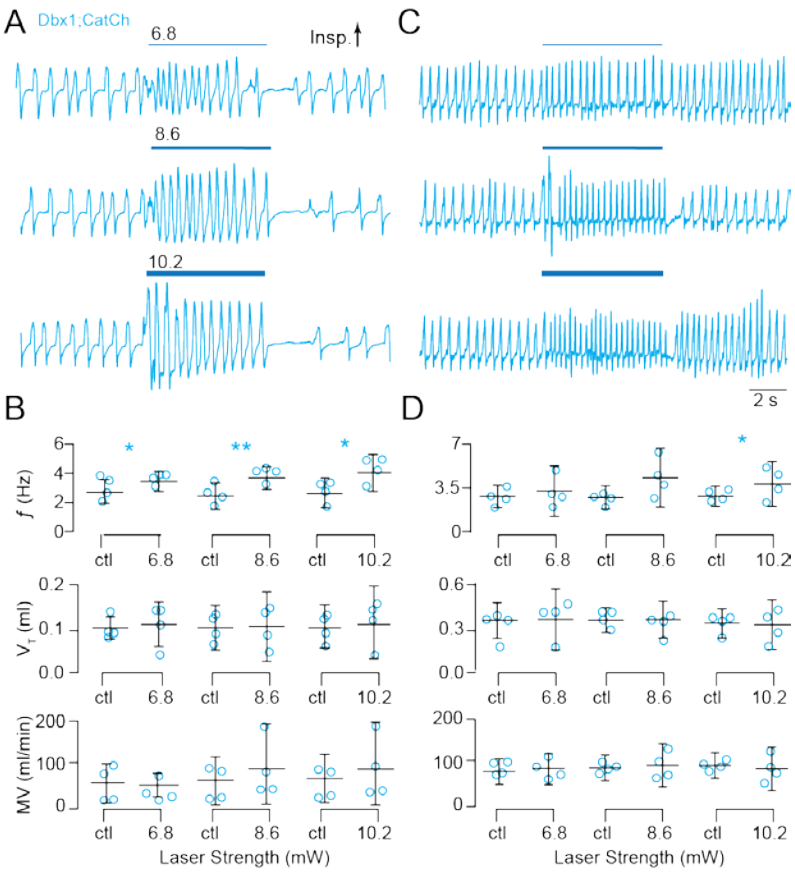

Figure 4. Photostimulation of Dbx1 preBötC neurons speeds-up breathing in adult Dbx1;CatCh mice. **A**, Airflow traces from a sedated mouse exposed to 5-s bouts of unilateral preBötC illumination at three intensities (units of mW). Cyan line thickness corresponds to light intensity, which is also annotated above each line. **B**, Group data from experiments in A quantifying light-evoked changes in f, V_T and MV. Symbols show the mean f, V_T, and MV measured in each mouse. Bars show the mean and SD for all animals tested (n = 4). Control measurements are labeled 'ctl'; numerals indicate light intensity. **C**, Airflow traces from an awake unrestrained mouse exposed to 5-s bouts of bilateral preBötC illumination at three intensities. Cyan line thickness corresponds to light intensity; annotations mach those in A. **D**, Group data from experiments in C quantifying light-evoked changes in f, V_T and MV. Symbols show the mean f, V_T, and MV measured in each mouse. Bars show the mean and SD for all animals tested (n = 4). Control measurements are labeled 'ctl'; numerals indicate light intensity. Asterisks represent statistical significance at $p < 0.05$; the double asterisk represents $p < 0.01$.

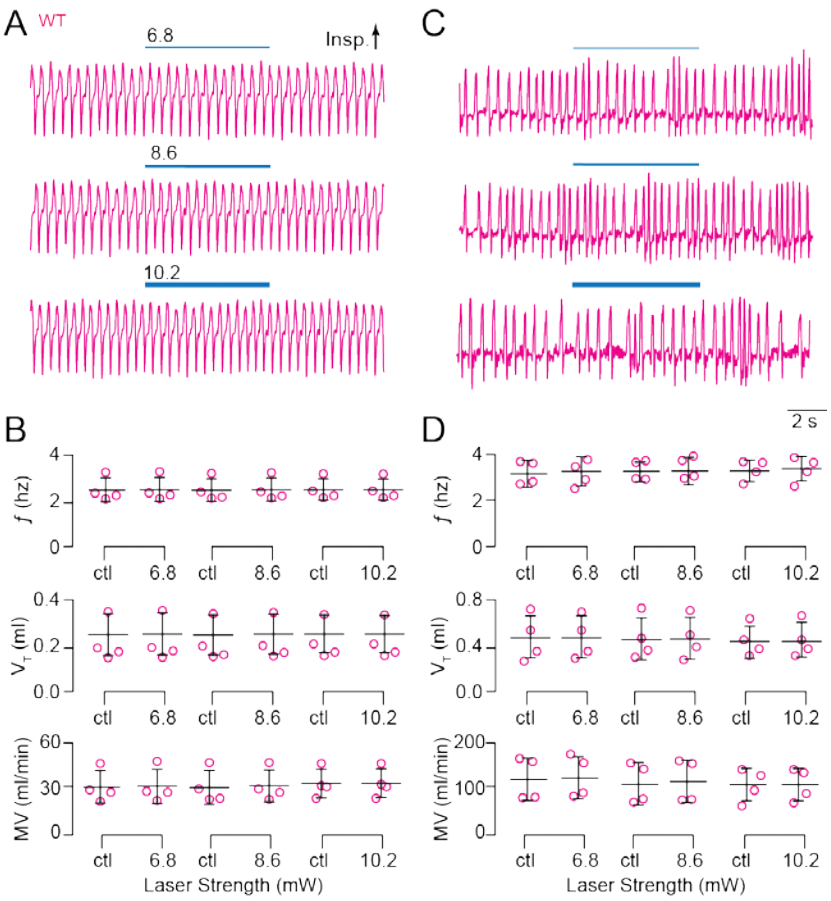

Figure 4 – figure supplement 1. Light application to the preBötC does not affect breathing in wild type Dbx1;CatCh littermates. **A**, Airflow traces from a sedated mouse exposed to 5-s bouts of unilateral preBötC illumination at three intensities (units of mW). Cyan line thickness corresponds to light intensity, which is also annotated above each line. **B**, Group data from experiments in A quantifying f, V_T and MV in response to light application. Symbols show mean f, V_T, and MV in each mouse. Bars show the mean and SD for all animals tested (n = 4). Control measurements are labeled 'ctl'. **C**, Traces from an awake unrestrained mouse exposed to 5-s bouts of unilateral preBötC illumination at three intensities. Cyan line thickness corresponds to light intensity; annotations mach those in A. **D**, Group data from experiments in C quantifying f, V_T and MV in response to light application. Symbols show mean f, V_T, and MV in each mouse. Bars show the mean and SD for all animals tested (n = 6). Control measurements are labeled 'ctl'; numerals indicate light intensity.

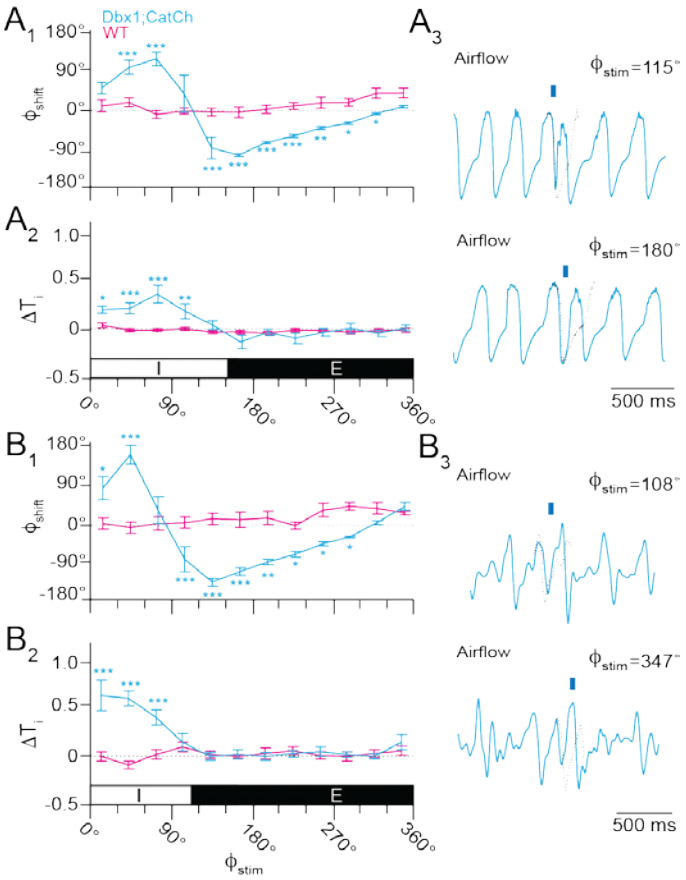

Figure 5. Effects of brief photostimulation on the breathing phase and inspiratory duration from Dbx1;CatCh mice (n = 4, cyan) and wild type littermates (n = 4, magenta). **A_1**, Phase-response curve plotting Φ_{Shift} following 100-ms photostimulation at Φ_{Stim} throughout the breathing cycle in sedated mice. Φ_{Stim} was partitioned into 12 equally sized bins (30º) in A and B. **A_2**, Phase-response curve for changes in T_i following photostimulation (i.e., the perturbed breath) in the same cohort of sedated mice. The abscissa marks the inspiratory (I, 0-150º) and expiratory (E, 150-360º) phases of the breathing cycle (0-360º), which applies to A_1 and A_2. **A_3**, Sample airflow traces from a representative sedated mouse (Φ_{Stim} is indicated by an orange bar and numeral value). Time calibration as shown. **B_1**, Phase-response curve plotting Φ_{Shift} following brief photostimulation at Φ_{Stim} throughout the breathing cycle in awake unrestrained mice. **B_2**, Phase-response curve for changes in T_i following brief photostimulation (i.e., the perturbed breath) in the same cohort of awake unrestrained mice. The abscissa marks the inspiratory (I, 0-110º) and expiratory (E, 110-360º) phases of the complete breathing cycle (0-360º), which applies to B_1 and B_2. **B_3**, Sample airflow traces from a representative awake unrestrained mouse (Φ_{Stim} is indicated by an orange bar and numeral value). Time calibration is shown.

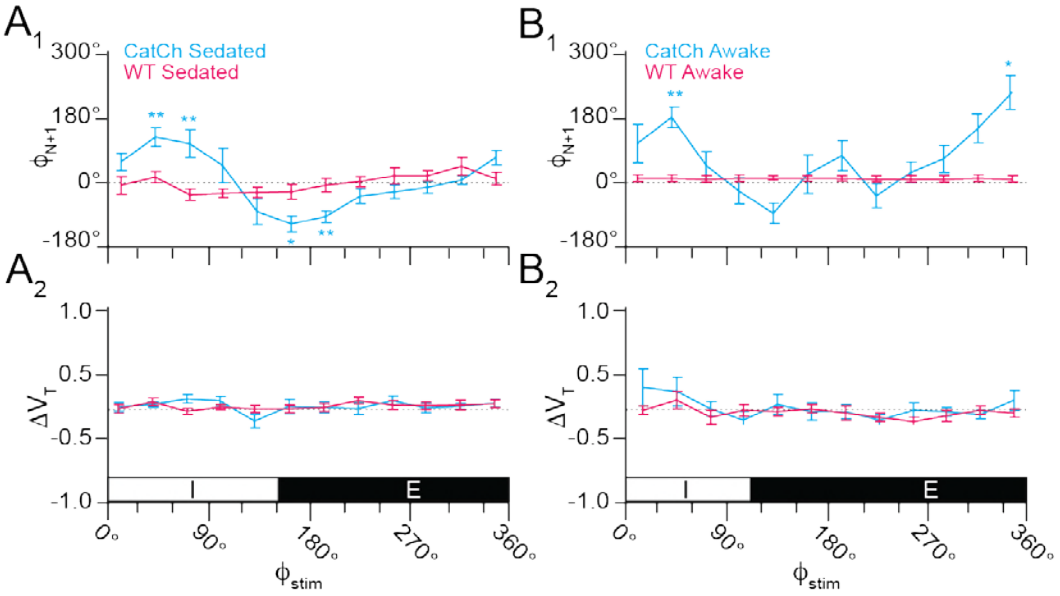

Figure 5 – figure supplement 1. Effects of brief photostimulation on V_T and Φ_{N+1} in Dbx1;CatCh mice (n = 4, cyan) or wild type littermates (n = 4, magenta). **A_1**, Phase-response curve plotting Φ_{N+1} vs. Φ_{Stim} throughout the breathing cycle in sedated mice. **A_2**, Phase-response curve for changes in V_T following photostimulation (i.e., the perturbed breath) in the same cohort of sedated mice (n = 4). The abscissa marks the inspiratory (I, 0-150º) and expiratory (E, 150-360º) phases of the breathing cycle (0-360º), which applies to A_1 and A_2. **B_1**, Phase-response curve plotting Φ_{N+1} vs. Φ_{Stim} in awake unrestrained mice. **B_2**, Phase-response curve for ΔV_T vs. Φ_{Stim} in the same cohort of awake unrestrained mice. The abscissa marks the inspiratory (I, 0-110º) and expiratory (E, 110-360º) phases of the complete breathing cycle (0-360º), which applies to B_1 and B_2.